NUWC-NPT Technical Report 11,093
5 February 1996

An Inverse Method to Measure the Breathing Wave Speed in a Liquid-Filled Cylindrical Shell

Andrew J. Hull
Submarine Sonar Department

Naval Undersea Warfare Center Division
Newport, Rhode Island

PREFACE

The investigation described in this report was sponsored by the Office of Naval Research in Arlington, Virginia.

The technical reviewer for this report was B. M. Abraham (Code 2141).

The author wishes to thank K. A. Holt (Code 5131) for her help with the editing of the manuscript.

Reviewed and Approved: 5 February 1996

R. J. Martin
Acting Head, Submarine Sonar Department

REPORT DOCUMENTATION PAGE

Form Approved
OMB No. 0704-0188

1. AGENCY USE ONLY (Leave Blank)	2. REPORT DATE	3. REPORT TYPE AND DATES COVERED
	5 February 1996	Final

4. TITLE AND SUBTITLE

An Inverse Method to Measure the Breathing Wave Speed in a Liquid-Filled Cylindrical Shell

5. FUNDING NUMBERS

6. AUTHOR(S)

Andrew J. Hull

7. PERFORMING ORGANIZATION NAME(S) AND ADDRESS(ES)

Naval Undersea Warfare Center
Detachment New London
New London, Connecticut 06320

8. PERFORMING ORGANIZATION REPORT NUMBER

TR 11,093

9. SPONSORING/MONITORING AGENCY NAME(S) AND ADDRESS(ES)

Office of Naval Research
800 North Quincy Street
Arlington, VA 22217

10. SPONSORING/MONITORING AGENCY REPORT NUMBER

11. SUPPLEMENTARY NOTES

12a. DISTRIBUTION/AVAILABILITY STATEMENT

Approved for public release; distribution is unlimited.

12b. DISTRIBUTION CODE

13. ABSTRACT (Maximum 200 words)

An inverse method is developed for measuring the breathing wave speed in a liquid-filled cylindrical shell. The model used with this method is based on an experimental configuration in which a long cylindrical shell is longitudinally excited by a mechanical shaker at one end. The resulting longitudinal wave propagation produces a spatial field in the shell that consists of extensional and breathing waves. End-mounted accelerometers and force transducers are used to measure the extensional wave speed. Once this is accomplished, transfer functions between five equally spaced hydrophones (in the fluid) and a forward accelerometer are recorded. These data are then combined to yield a closed form value of the complex, frequency-dependent breathing wave speed. The experiment included to validate this method is extremely easy to implement and can be rapidly executed.

14. SUBJECT TERMS

Breathing Wave Speed, Cylindrical Shell, Extensional Wave Speed, Inverse Method, Liquid-Filled Shell

15. NUMBER OF PAGES

30

16. PRICE CODE

17. SECURITY CLASSIFICATION OF REPORT	18. SECURITY CLASSIFICATION OF THIS PAGE	19. SECURITY CLASSIFICATION OF ABSTRACT	20. LIMITATION OF ABSTRACT
UNCLASSIFIED	**UNCLASSIFIED**	**UNCLASSIFIED**	**SAR**

TABLE OF CONTENTS

LIST OF ILLUSTRATIONS

AN INVERSE METHOD TO MEASURE THE BREATHING WAVE SPEED IN A LIQUID-FILLED CYLINDRICAL SHELL

1. INTRODUCTION

The breathing (or bulge) wave is a fluid-solid interaction wave that propagates in liquid-filled shells [1], and its wave speed is typically modeled as a complex, frequency-dependent quantity. This wave can be generated by applying axial excitation to one or both ends of the shell. Breathing and extensional wave motion is initiated at the location of this excitation, and both of these waves propagate longitudinally in the structure. Additionally, the shell ends reflect such wave motion, and the shell domain dissipates some of the energy, creating a spatial field composed of partially standing and partially propagating waves. This wave motion causes a change in the cross-sectional area of the shell, which creates a pressure differential in the fluid. The amplitude of this fluid pressure is used to measure the breathing wave, which is strong at lower frequencies (typically below 20 Hz for most end-vibrated, liquid-filled shells). A previous technique to measure breathing wave speed [2] resulted in a single frequency measurement that did not include the loss (imaginary) term of the wave. Additionally, this method required sensors near the endcap of the shell, which is an area that is very susceptible to acoustic scattering.

In this report, an inverse method is derived to measure the breathing wave speed of liquid-filled shells. First, the governing wave equation for particle motion is solved to yield a model of the displacement and force in the shell. The force and displacement equations are then written to correspond to two sensor transfer functions. These two equations and their corresponding data are now combined, resulting in a closed-form value of the extensional wave speed (including a loss term) at each frequency where a measurement was made. Next, two governing wave equations for fluid pressure are solved to produce a model of the pressure in the shell. The pressure equation is then written to correspond to the transfer functions between five equally spaced hydrophones (in the fluid) and a forward-mounted accelerometer. These

five equations and their corresponding data are combined to yield a closed-form value of the breathing wave speed (including a loss term). The breathing wave speed measurement is to be made at low frequencies where the breathing wave is spatially coherent across the length of the shell. The amplitude of the breathing wave at higher frequencies is extremely small and coherent wavelengths do not exist; thus no high frequency measurements of this wave are made. This approach is intended for use in the Axial Vibration Test Facility (AVTF) at the Naval Undersea Warfare Center (NUWC), Detachment New London, where liquid-filled shells are tested, typically under a tensile load.

2. EXTENSIONAL WAVE SPEED MEASUREMENT

In order to measure the breathing wave speed, it is necessary to know the extensional wave speed. This complex, frequency-dependent quantity is determined using the measurements from the forward and aft impedance heads in the AVTF [3]. Although these measurements contain a breathing wave contribution, it typically occurs only at low frequencies and can be discerned from the extensional wave effects with this method. This behavior is discussed in the experiment section.

The governing differential equation of the extensional wave is expressed on the spatial domain as a single wave equation with particle displacement as the independent variable:

$$\frac{d^2U(x,\omega)}{dx^2} + k_e^2 U(x,\omega) = 0 \ , \tag{1}$$

where $U(x,\omega)$ is the temporal Fourier transform of the axial displacement, x is the spatial location (m), ω is the frequency of excitation (rad/s), and k_e is the complex extensional wavenumber of the shell (rad/m). It is implicit in equation (1) that the fluid-loading effects of the extensional wave speed are incorporated in the axial model of the shell with a homogeneous medium that supports longitudinal wave motion. Although this approximation is not sufficient to model the radial motion of the shell, it is an accurate model of axial motion and its corresponding extensional wave propagation. The extensional wavenumber is equal to

$$k_e = \frac{\omega}{c_e} , \tag{2}$$

where c_e is the complex extensional (longitudinal) wave speed of the shell (m/s). The energy attenuation in the shell is defined with a structural damping law, and therefore the wave speed is a complex quantity. The real part of the wave speed corresponds to energy transmission and the imaginary part corresponds to energy attenuation.

The solution to equation (1) is

$$U(x,\omega) = Ge^{ik_e x} + He^{-ik_e x} , \tag{3}$$

where G and H are coefficients determined by the boundary conditions at the ends of the shell and i is the square root of -1. It is not necessary to know these boundary conditions to determine the longitudinal wave speed of the shell. The temporal Fourier transform of the axial force in the shell is

$$F(x,\omega) = A_s E_x \frac{dU(x,\omega)}{dx} = A_s E_x i k_e \left(Ge^{ik_e x} - He^{-ik_e x} \right) , \tag{4}$$

where A_s is the cross-sectional area of the shell (m^2) and E_x is the effective longitudinal modulus of the shell (N/m^2). The known parameters in equations (3) and (4) are the location of the sensors (x) and the frequency of excitation (ω). Although the effective longitudinal modulus (E_x) is unknown, equation (4) will be rewritten as a ratio of forces permitting the cancellation of this term and the cross-sectional area (A_s). The inversion of equations (3) and (4) at the sensor locations will allow for a measurement of the unknown extensional wave speed c_e. This technique is described next.

The extensional wave measurement part of the experiment has a forward and aft pair of sensors to collect data that are in the form of transfer functions between each pair. The position of the forward pair is defined as $x = 0$ and of the aft pair as $x = L$, where L is the length of the shell (m). The two transfer function measurements used are the forward displacement divided by the aft displacement and the forward force divided by the aft force. Their theoretical form can be rewritten using equations (3) and (4) as

$$\frac{U(0,\omega)}{U(L,\omega)} = \frac{G+H}{Ge^{ik_eL} + He^{-ik_eL}} = R_1 \tag{5}$$

and

$$\frac{F(0,\omega)}{F(L,\omega)} = \frac{G-H}{Ge^{ik_eL} - He^{-ik_eL}} = R_2 \ , \tag{6}$$

where R_1 and R_2 are transfer function data from the experiment. Equations (5) and (6) are rewritten as functions of *H*/*G* and are set equal to each other, yielding

$$\cos(k_eL) = \frac{R_2R_1 + 1}{R_2 + R_1} = \phi \ , \tag{7}$$

where ϕ is a complex quantity. Using an angle-sum relationship on the complex cosine term in equation (7) and separating the equation into real and imaginary parts results in

$$\cosh[\mathrm{Im}(k_e)L] = \frac{\mathrm{Re}(\phi)}{\cos[\mathrm{Re}(k_e)L]} \tag{8}$$

and

$$\sinh[\mathrm{Im}(k_e)L] = \frac{-\mathrm{Im}(\phi)}{\sin[\mathrm{Re}(k_e)L]} \ , \tag{9}$$

where Re denotes the real part and Im denotes the imaginary part of the corresponding complex quantity.

Equation (9) is now squared and subtracted from the square of equation (8), yielding

$$\left\{\cosh[\mathrm{Im}(k_e)L]\right\}^2 - \left\{\sinh[\mathrm{Im}(k_e)L]\right\}^2 = \frac{[\mathrm{Re}(\phi)]^2}{\left\{\cos[\mathrm{Re}(k_e)L]\right\}^2} - \frac{[\mathrm{Im}(\phi)]^2}{\left\{\sin[\mathrm{Re}(k_e)L]\right\}^2} = 1 \ . \tag{10}$$

Equation (10) can be simplified using trigonometric power relationships to

$$\cos[2\,\mathrm{Re}(k_e)L] =$$

$$[\mathrm{Re}(\phi)]^2 + [\mathrm{Im}(\phi)]^2 - \sqrt{\left([\mathrm{Re}(\phi)]^2 + [\mathrm{Im}(\phi)]^2\right)^2 - \left(2[\mathrm{Re}(\phi)]^2 - 2[\mathrm{Im}(\phi)]^2 - 1\right)} = s \ . \tag{11}$$

Note that only a negative sign in front of the radical is used. The real part of k_e in equation (11) is now solved for by

$$\mathrm{Re}(k_e) = \begin{cases} \dfrac{1}{2L}\mathrm{Arc}\cos(s) + \dfrac{n\pi}{2L} & n \text{ even} \\ \dfrac{1}{2L}\mathrm{Arc}\cos(-s) + \dfrac{n\pi}{2L} & n \text{ odd} \end{cases}, \tag{12}$$

where n is a nonnegative integer and the capital A denotes the principal value of the inverse cosine function. The value of n is determined from the function s, which is a cosine function with respect to frequency. At zero frequency, n is 0. Every time s cycles through π radians, n is increased by 1. The imaginary part of k_e is determined by adding equations (8) and (9) together, resulting in

$$\mathrm{Im}(k_e) = \frac{1}{L}\log_e\left\{\frac{\mathrm{Re}(\phi)}{\cos[\mathrm{Re}(k_e)L]} - \frac{\mathrm{Im}(\phi)}{\sin[\mathrm{Re}(k_e)L]}\right\}. \tag{13}$$

Now that the real and imaginary parts of the wavenumber k_e are known, the complex-valued extensional wave speed can be determined at each frequency with

$$c_e = \mathrm{Re}(c_e) + i\,\mathrm{Im}(c_e) = \frac{\omega}{k_e}. \tag{14}$$

Note that the extensional wave speed has been measured without knowing the boundary conditions at $x = 0$ and $x = L$.

3. BREATHING WAVE SPEED MEASUREMENT

The pressure field inside the fluid-filled shell is used to measure the breathing wave speed. The dynamic model of this field is derived from two wave equations in the spatial domain, both of which use pressure as the independent variable. The first equation models the extensional wave contribution and is written as

$$\frac{d^2P_e(x,\omega)}{dx^2} + k_e^2 P_e(x,\omega) = 0, \tag{15}$$

where $P_e(x,\omega)$ is the temporal Fourier transform of the pressure that is generated by the extensional wave and k_e is the extensional wavenumber that was determined using the method

in section 2. The second wave equation models the breathing wave contribution and is written as

$$\frac{d^2 P_b(x,\omega)}{dx^2} + k_b^2 P_b(x,\omega) = 0 \ , \tag{16}$$

where $P_b(x,\omega)$ is the temporal Fourier transform of the pressure that is generated by the breathing wave and k_b is the complex breathing wavenumber (rad/m), which is equal to

$$k_b = \frac{\omega}{c_b} \ , \tag{17}$$

where c_b is the complex breathing wave speed (m/s). The solutions to equations (15) and (16) are similar to equation (3), and they can be added together using the principle of superposition, which yields the total pressure in the shell as

$$P(x,\omega) = P_e(x,\omega) + P_b(x,\omega) = \overline{A} e^{ik_e x} + \overline{B} e^{-ik_e x} + \overline{C} e^{ik_b x} + \overline{D} e^{-ik_b x} \ , \tag{18}$$

where $P(x,\omega)$ is the temporal Fourier transform of the pressure that is generated by both the extensional wave and the breathing wave, and $\overline{A}$, $\overline{B}$, $\overline{C}$, and $\overline{D}$ are wave propagation coefficients determined by the boundary conditions. It is now noted that the pressure field at x divided by the forward accelerometer is

$$\frac{P(x,\omega)}{\ddot{U}} = A e^{ik_e x} + B e^{-ik_e x} + C e^{ik_b x} + D e^{-ik_b x} \ , \tag{19}$$

where $\ddot{U}$ is the temporal Fourier transform of the forward accelerometer; A, B, C, and D are wave propagation coefficients; and $P(x,\omega)/\ddot{U}$ has units of μPa/g. It is not necessary to know the values of A through D to determine the breathing wave speed, as they will be extracted from the manipulated governing equations. Five independent measurements of the spatial pressure field are needed to eliminate these wave propagation coefficients and solve for the breathing wave speed. Without loss of generality, the origin of the coordinate system is defined as $x = 0$ at the middle (third) pressure sensor (hydrophone). Equation (19) is written to correspond to the locations of the five pressure sensors as

$$\frac{P(-2\delta,\omega)}{\ddot{U}} = Ae^{-ik_e 2\delta} + Be^{ik_e 2\delta} + Ce^{-ik_b 2\delta} + De^{ik_b 2\delta} = S_1 \ , \tag{20}$$

$$\frac{P(-\delta,\omega)}{\ddot{U}} = Ae^{-ik_e \delta} + Be^{ik_e \delta} + Ce^{-ik_b \delta} + De^{ik_b \delta} = S_2 \ , \tag{21}$$

$$\frac{P(0,\omega)}{\ddot{U}} = A + B + C + D = S_3 \ , \tag{22}$$

$$\frac{P(\delta,\omega)}{\ddot{U}} = Ae^{ik_e \delta} + Be^{-ik_e \delta} + Ce^{ik_b \delta} + De^{-ik_b \delta} = S_4 \ , \tag{23}$$

and

$$\frac{P(2\delta,\omega)}{\ddot{U}} = Ae^{ik_e 2\delta} + Be^{-ik_e 2\delta} + Ce^{ik_b 2\delta} + De^{-ik_b 2\delta} = S_5 \ , \tag{24}$$

where δ is the sensor-to-sensor spacing (m) and S_1 through S_5 correspond to the measured transfer function data.

Equations (21) and (23) are now added together to yield

$$(A+B)\cos(k_e\delta) + (C+D)\cos(k_b\delta) = (1/2)(S_2 + S_4) \ , \tag{25}$$

and equations (20) and (24) are added together to produce

$$(A+B)\cos(k_e 2\delta) + (C+D)\cos(k_b 2\delta) = (1/2)(S_1 + S_5) \ . \tag{26}$$

Equation (22) is now rewritten with the term $(A + B)$ on the left-hand side and substituted into equations (25) and (26), yielding

$$C + D = \frac{(1/2)(S_2 + S_4) - S_3\cos(k_e\delta)}{\cos(k_b\delta) - \cos(k_e\delta)} \ . \tag{27}$$

and

$$C + D = \frac{(1/2)(S_1 + S_5) - S_3\cos(k_e 2\delta)}{\cos(k_b 2\delta) - \cos(k_e 2\delta)} \ , \tag{28}$$

respectively. Equations (27) and (28) are now set equal to each other. Applying a double angle trigonometric relationship to the $\cos(k_b 2\delta)$ term then produces

$$X\cos^2(k_b\delta) + Y\cos(k_b\delta) + Z = 0 \ , \tag{29a}$$

where

$$X = (S_2 + S_4) - 2S_3 \cos(k_e \delta) \quad , \tag{29b}$$

$$Y = S_3 \cos(k_e \delta) - (1/2)(S_1 + S_5) \quad , \tag{29c}$$

and

$$Z = [(1/2)(S_1 + S_5) + S_3]\cos(k_e \delta) - (1/2)(S_2 + S_4)\cos(k_e 2\delta) - (1/2)(S_2 + S_4) \quad . \tag{29d}$$

Equation (29) is a quadratic form with solution

$$\cos(k_b \delta) = \frac{-Y \pm \sqrt{Y^2 - 4XZ}}{2X} = \psi \quad , \tag{30}$$

where ψ is a complex quantity. Equation (30) is similar to equation (7) and the corresponding solution is

$$\cos[2\,\mathrm{Re}(k_b)\delta] =$$

$$[\mathrm{Re}(\psi)]^2 + [\mathrm{Im}(\psi)]^2 - \sqrt{\left([\mathrm{Re}(\psi)]^2 + [\mathrm{Im}(\psi)]^2\right)^2 - \left(2[\mathrm{Re}(\psi)]^2 - 2[\mathrm{Im}(\psi)]^2 - 1\right)} = r \quad . \tag{31}$$

Note that only a negative sign in front of the radical is used in equation (31). However, both the negative and the positive signs in front of the radical in equation (30) are needed. The real part of k_b in equation (31) is now solved for by

$$\mathrm{Re}(k_b) = \begin{cases} \dfrac{1}{2\delta}\mathrm{Arc}\cos(r) + \dfrac{m\pi}{2\delta} & m \text{ even} \\ \dfrac{1}{2\delta}\mathrm{Arc}\cos(-r) + \dfrac{m\pi}{2\delta} & m \text{ odd} \end{cases} \quad , \tag{32}$$

where m is a nonnegative integer and the capital A denotes the principal value of the inverse cosine function. The value of m is determined from the function r, which is a cosine function with respect to frequency. At zero frequency, m is 0. Every time r cycles through π radians, m is increased by 1. The imaginary part of k_b is determined in a manner similar to equation (13), resulting in

$$\mathrm{Im}(k_b) = \frac{1}{\delta}\log_e\left\{\frac{\mathrm{Re}(\psi)}{\cos[\mathrm{Re}(k_b)\delta]} - \frac{\mathrm{Im}(\psi)}{\sin[\mathrm{Re}(k_b)\delta]}\right\} \quad . \tag{33}$$

Now that the real and imaginary parts of the wavenumber k_b are known, the complex-valued breathing wave speed can be determined at each frequency with

$$c_b = \mathrm{Re}(c_b) + i\,\mathrm{Im}(c_b) = \frac{\omega}{k_b} \ . \tag{34}$$

Using this method produces two wave speed measurements because of the retention of the positive and negative signs in equation (30). One of the wave speeds is the breathing wave speed, and the other is the extensional wave speed, which was previously arrived at using the method in section 2. The extensional wave speed is typically at least one order of magnitude greater than the breathing wave speed.

4. EXPERIMENT

Use of this model with the inverse method corresponds to the physical testing configuration in the AVTF, as shown in figure 1. The AVTF has been designed to provide a simple procedure for testing long structures under varying tensions and temperatures. The longitudinal shaker at the forward end of the structure provides axial excitation to the structure. A rope attached to the aft end of the structure and a winch allows the tension to be adjusted. A mass is attached between the shell and the rope to increase the force levels and decrease the acceleration levels. This mass also produces an impedance change at the end of the bar that is sufficiently large to allow accurate modeling of the rope behavior by a spring and damper rather than by a continuous media expression. A rail from which thin Kevlar lines can be hung to provide lateral support to heavy or long test specimens runs the entire length of the facility. The entire unit is surrounded by an air-conditioned PVC duct to permit temperature-dependent testing. Impedance heads are attached to the forward and aft ends of the structure to collect data during a test. Each impedance head consists of a single axial force transducer and an accelerometer. Hydrophones in the fluid-filled shell collect additional data during the test. A load cell that measures the tension on the structure is located between the rope and the mass.

Equipment used in this experiment includes a Zonic Corporation model 1215-10-T-ZSP86 hydraulic shaker, two PCB Piezotronics model 348A accelerometers, two PCB Piezotronics model 233A force transducers, a Lebow model 31/3 load cell, and a Cordem Corporation model 1215-RMO tension drum.

In the first part of the experiment, which measures the extensional wave speed, a longitudinally reinforced fluid-filled urethane shell containing five equally spaced hydrophones was placed in tension, as shown in figure 1. The shell had a mean radius of 0.015 m and a thickness of 0.0028 m; the internal fluid had a density of 760 kg/m^3. The axial tension on the shell was 890 N and the stressed length was 12.0 m. The point mass had a weight of 13.6 kg. The data from the force transducers, accelerometers, and hydrophones were acquired in the time domain with a Hewlett Packard (HP) 3562 dynamic signal analyzer. The analyzer then Fourier transformed the raw data to the frequency domain to obtain the desired transfer functions. The test was run with a frequency range between 3 and 100 Hz.

Equations (5)-(14) were applied to the experimental test data taken with the force transducers and accelerometers, and the resulting extensional wave speed of the structure was found. Figure 2 is a plot of the magnitude and phase of the ratio of the forward force to the aft force at each measurement frequency and corresponds to R_1 in equation (5). Figure 3 is a plot of the forward accelerometer divided by the aft accelerometer versus frequency and corresponds to R_2 in equation (6). Figure 4 is the calculated extensional wave speed versus frequency. The solid line corresponds to the computed wave speed and the dashed line to the ordinary least square (OLS) straight-line fit. The OLS fit was applied to the data between 35 and 100 Hz to minimize the effect of the breathing wave interaction seen at lower frequencies. The resulting OLS fit was $c_e = 624.7 + 0.8f$ (m/s) for the real part and $c_e = 69.0 + 0.4f$ (m/s) for the imaginary part (where f is frequency in Hertz). These same values are used for the extensional wave speed in the following calculations in order to determine the breathing wave speed.

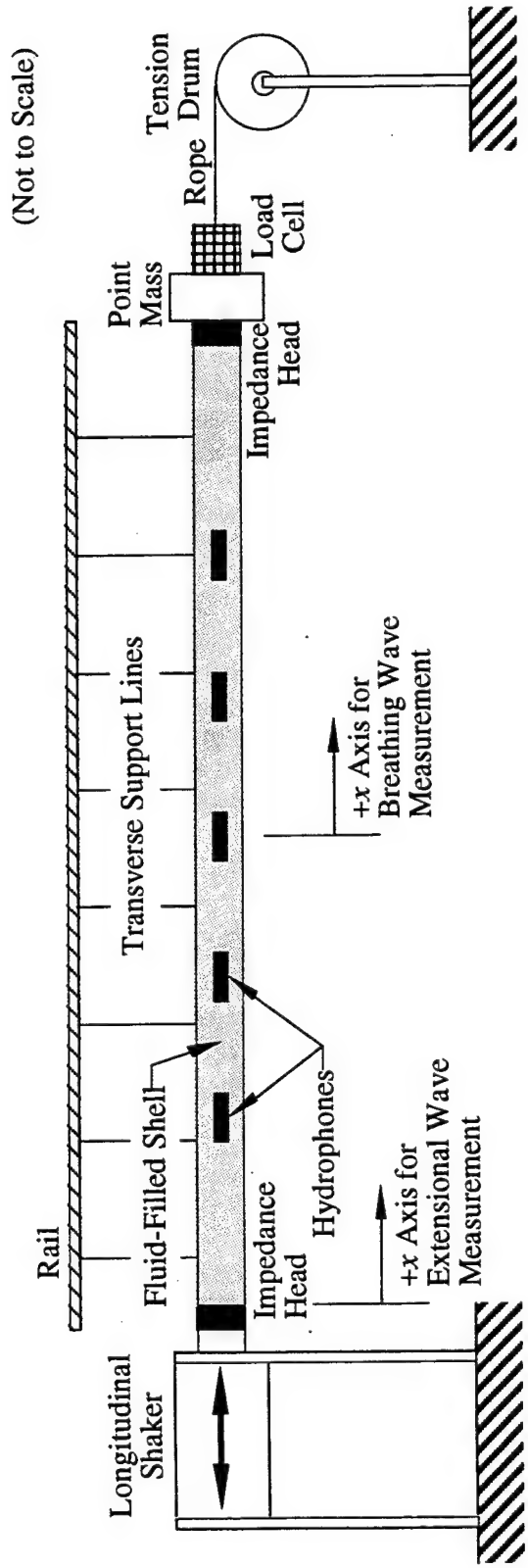

Figure 1. The Laboratory Configuration

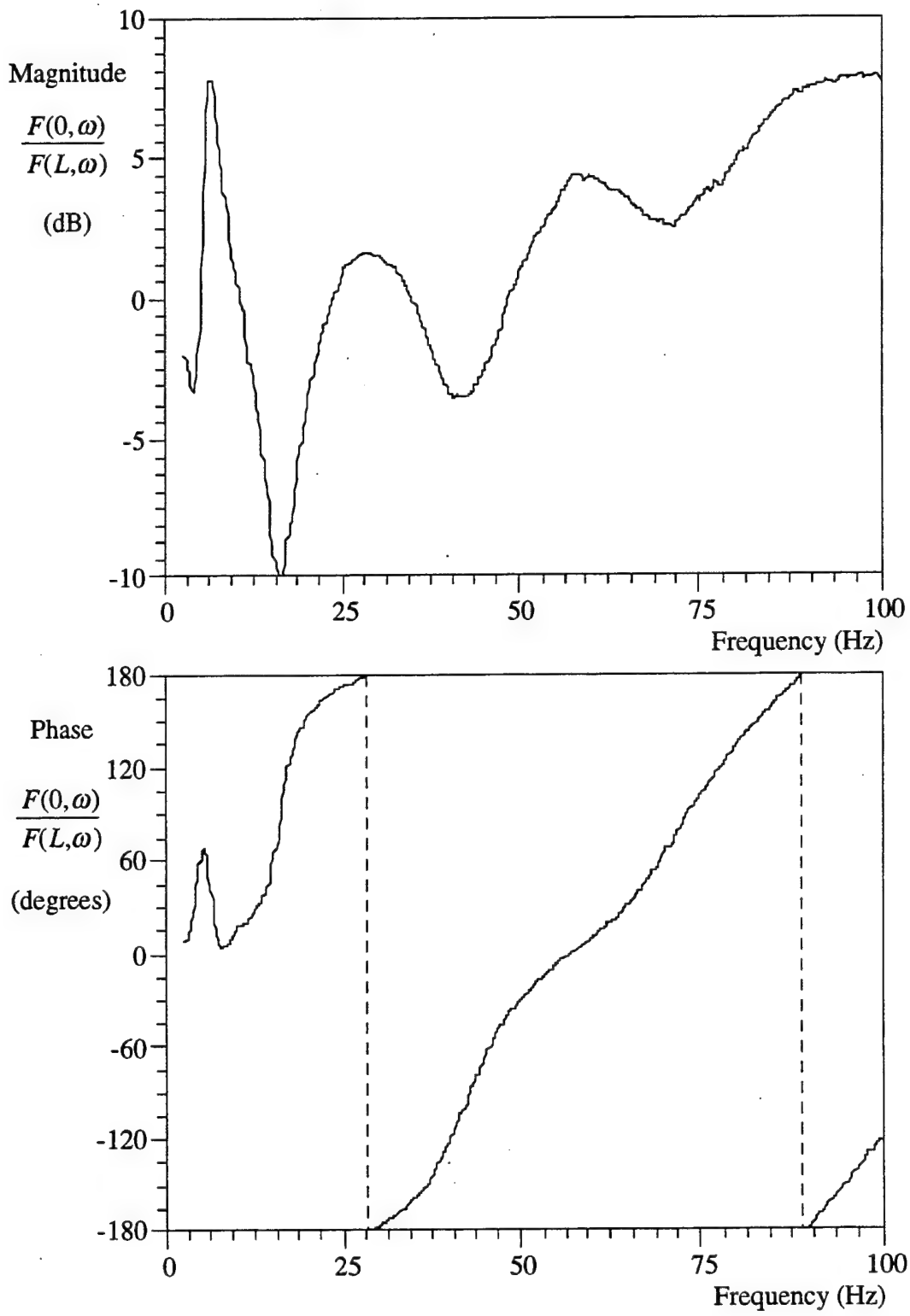

Figure 2. Transfer Function of Forward Force Divided by Aft Force Versus Frequency

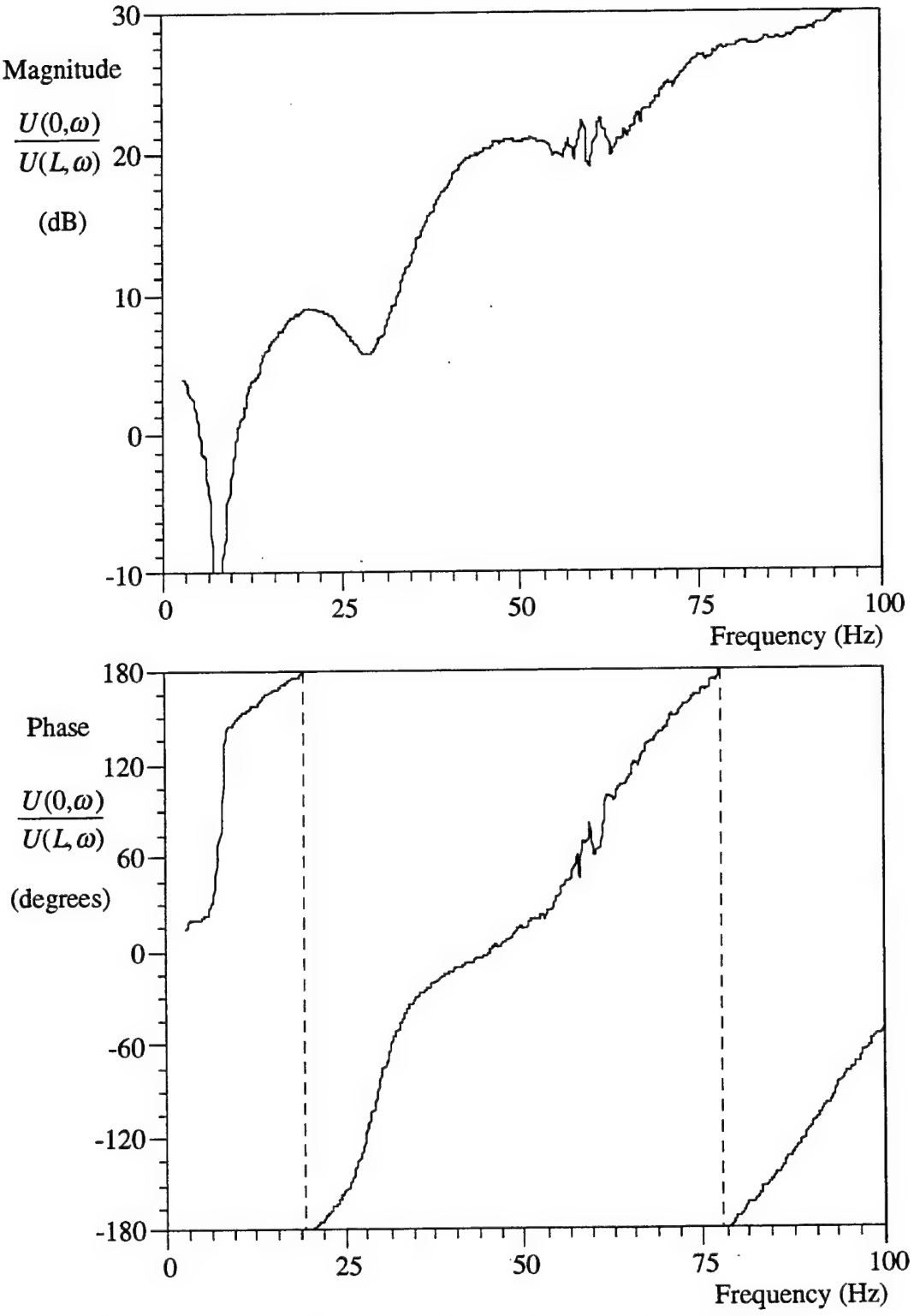

Figure 3. Transfer Function of Forward Displacement Divided by Aft Displacement Versus Frequency

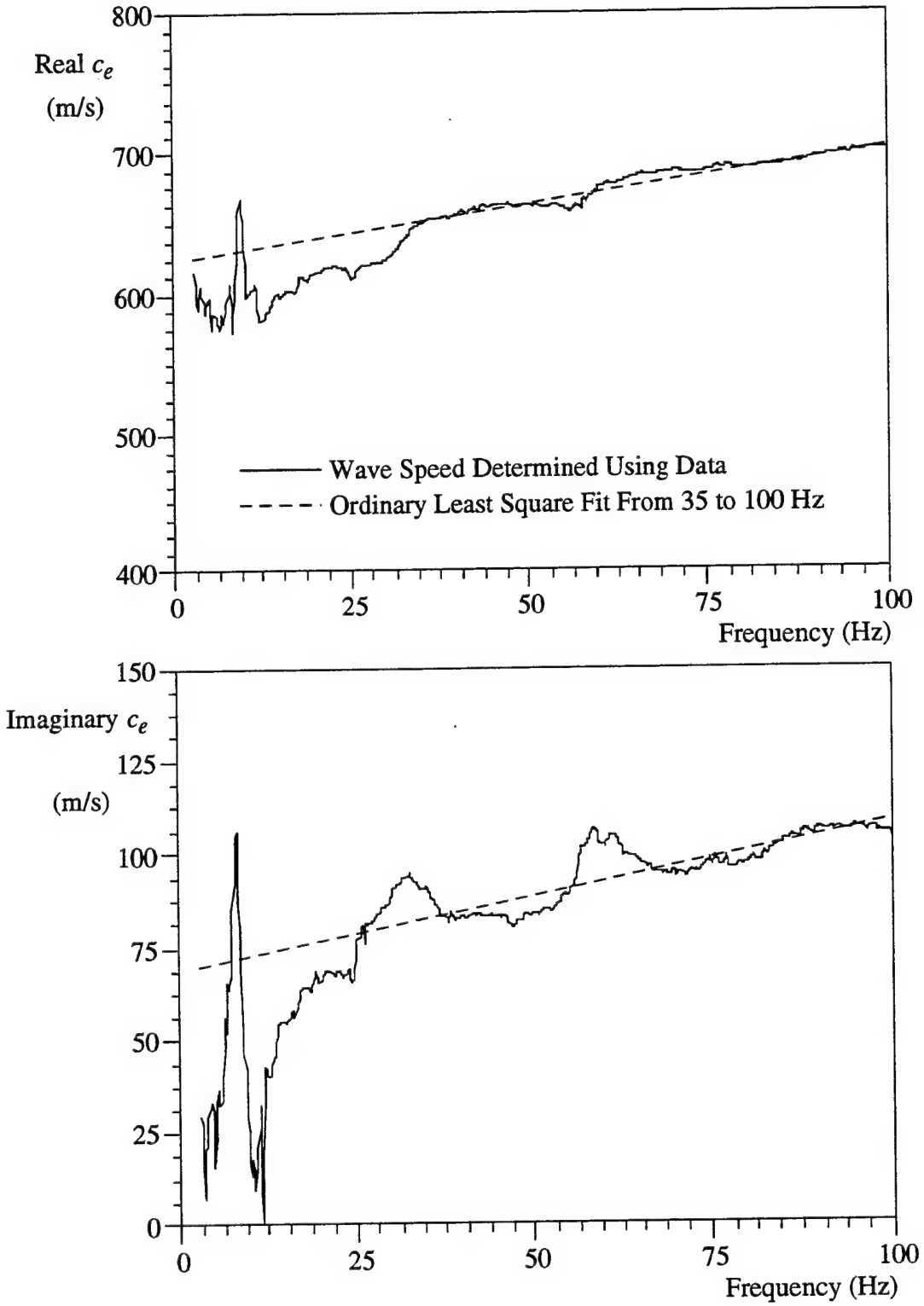

Figure 4. Extensional Wave Speed Versus Frequency

In the second part of the experiment, transfer function data of the hydrophones divided by the forward accelerometers were collected. The hydrophones were spaced at intervals of 1.83 m with a distance of 2.96 m from the forward end of the shell to the first hydrophone. Figures 5 through 9 are plots of the hydrophone pressure divided by the forward acceleration versus frequency and correspond to S_1 through S_5 in equations (20)-(24), respectively. Equations (25)-(34) were applied to the experimental test data, and the resulting breathing wave speed of the structure was calculated. Figure 10 is a plot of the breathing wave speed versus frequency. The plus symbols mark the data from this experiment that were obtained using the method developed in section 3. The two solid box symbols are data points determined with the phase angle between the forward accelerometer and the first hydrophone. This measurement is accomplished by first unwrapping the phase angle (of S_1) to a continuous function whose ordinate ranges from 0 to 1000 degrees. Next, regions that appear "straight" are identified. For these experimental data, the regions are 3 to 5 Hz and 10 to 25 Hz. An OLS line was fit to both regions, and a single (propagation) wave speed was determined using

$$c = d\frac{360\,\Delta f}{\Delta\theta}\,, \tag{35}$$

where c is the corresponding real wave speed (m/s), d is the distance between sensors (m), Δf is the change of frequency (Hz), and $\Delta\theta$ is the change of phase angle (degrees). The phase angle and corresponding straight-line fits are shown in figure 11. The region from 3 to 5 Hz resulted in a (real) breathing wave speed of 24.0 m/s and the region from 10 to 25 Hz resulted in a breathing wave speed of 54.8 m/s. The shortcomings of this "straight"-line calculation (equation (35)) are that it cannot incorporate extensional wave interaction, requires single direction wave propagation, allows for measurement of only the real part of the breathing wave speed, and is not a very objective test procedure. Additionally, it typically fails when the sensor-to-sensor separation distance is even moderately larger than that used in this experiment. However, it does provide a verification for the real part of the measured breathing wave speed.

In figure 10, it is noted that the breathing wave for this specific structure is spatially coherent from 3 to 13 Hz. Above 13 Hz, the imaginary part of the measurement begins to diverge. The spatial coherence length is related to the loss factor of the circumferential modulus of the shell. A smaller circumferential loss modulus would result in a longer spatial coherence length and a coherent measurement at higher frequencies. Respacing the hydrophone distances or use of a shorter shell might also result in coherent measurements at higher frequencies. Changing the extensional wave speed by ± 20 percent and recalculating the breathing wave speed produced a change in the breathing wave speed of less than 1 percent. Thus, the measurement method is very insensitive to incorrect extensional wave speeds.

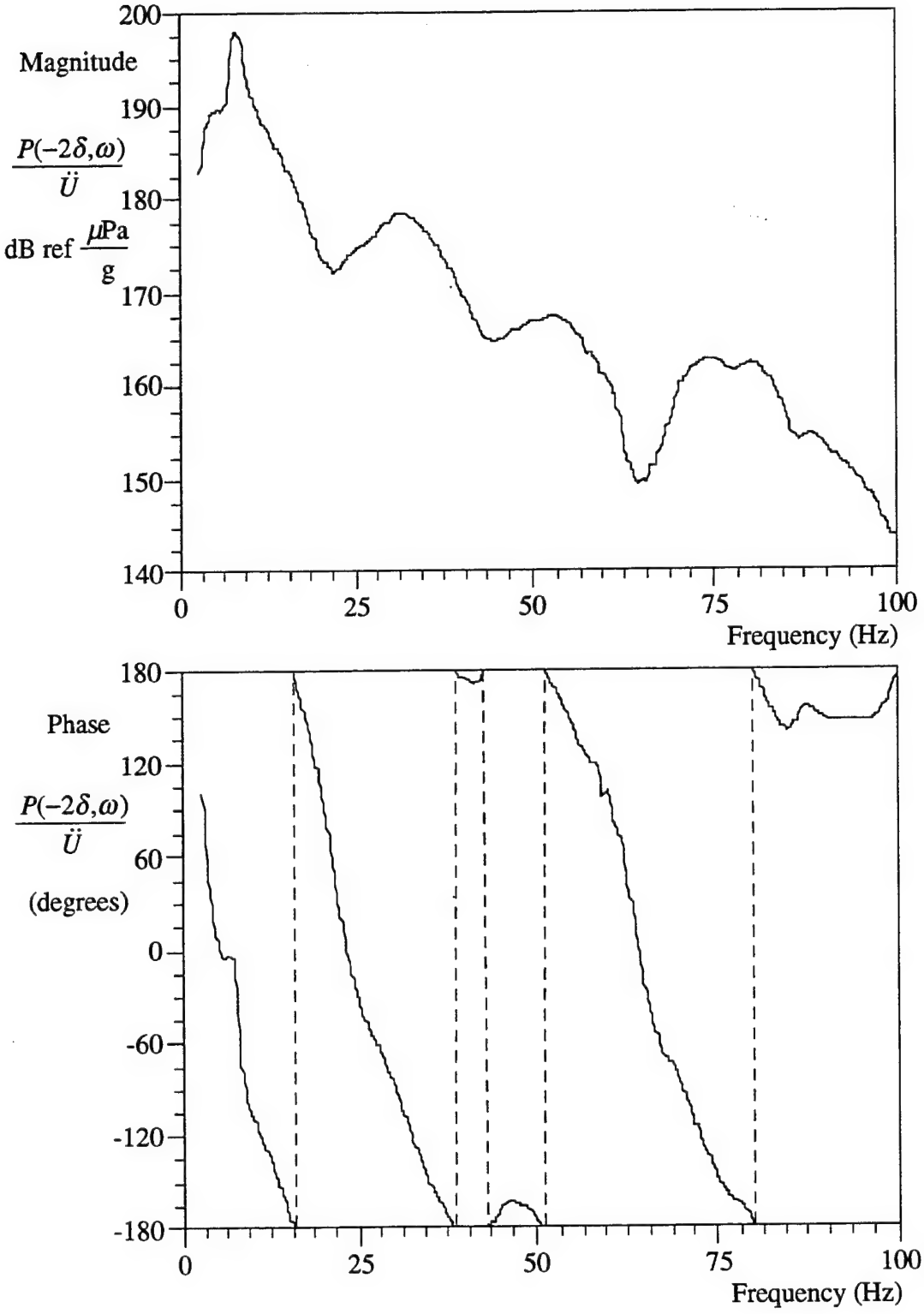

Figure 5. First Hydrophone Pressure Divided by Forward Acceleration Versus Frequency

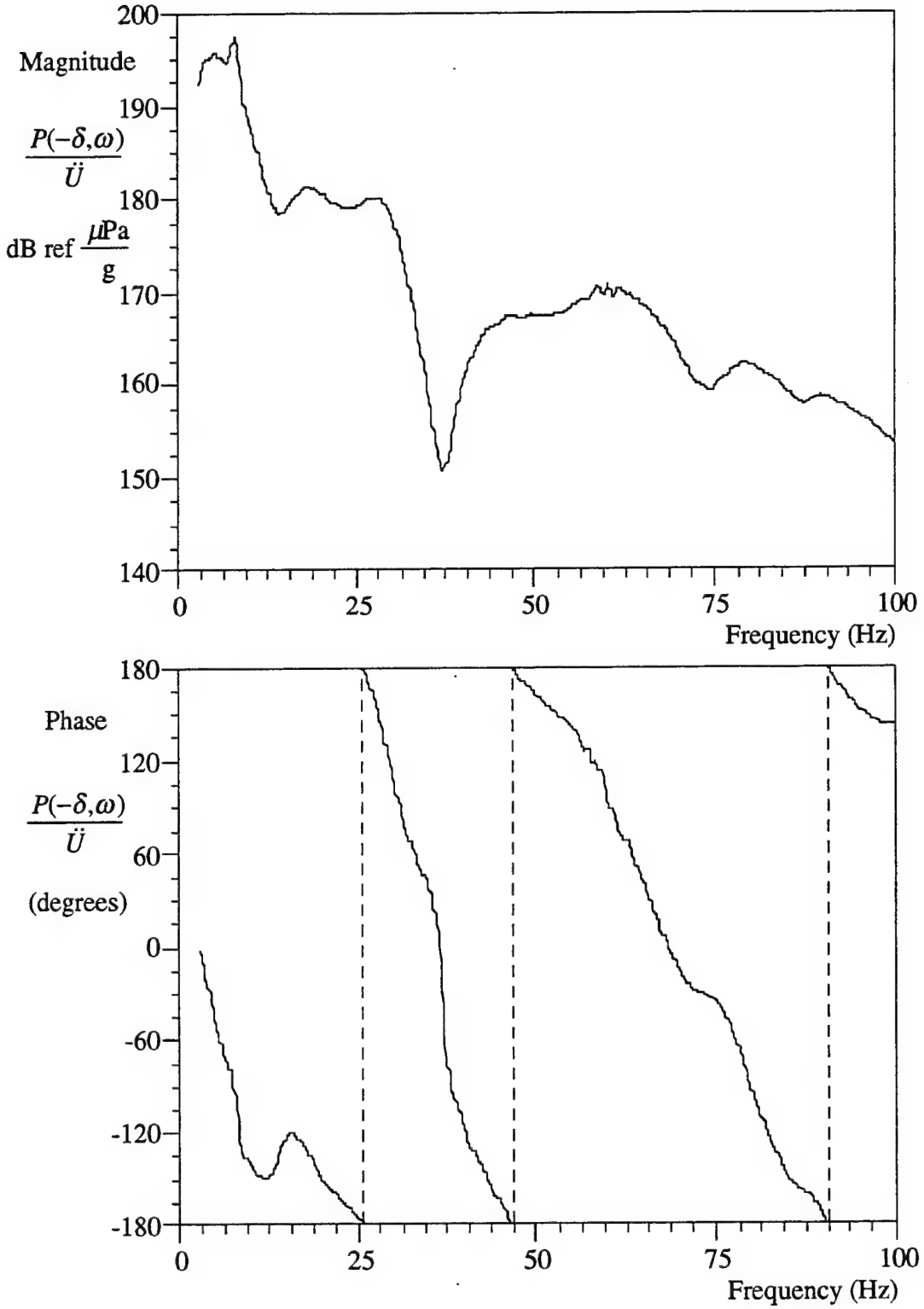

Figure 6. Second Hydrophone Pressure Divided by Forward Acceleration Versus Frequency

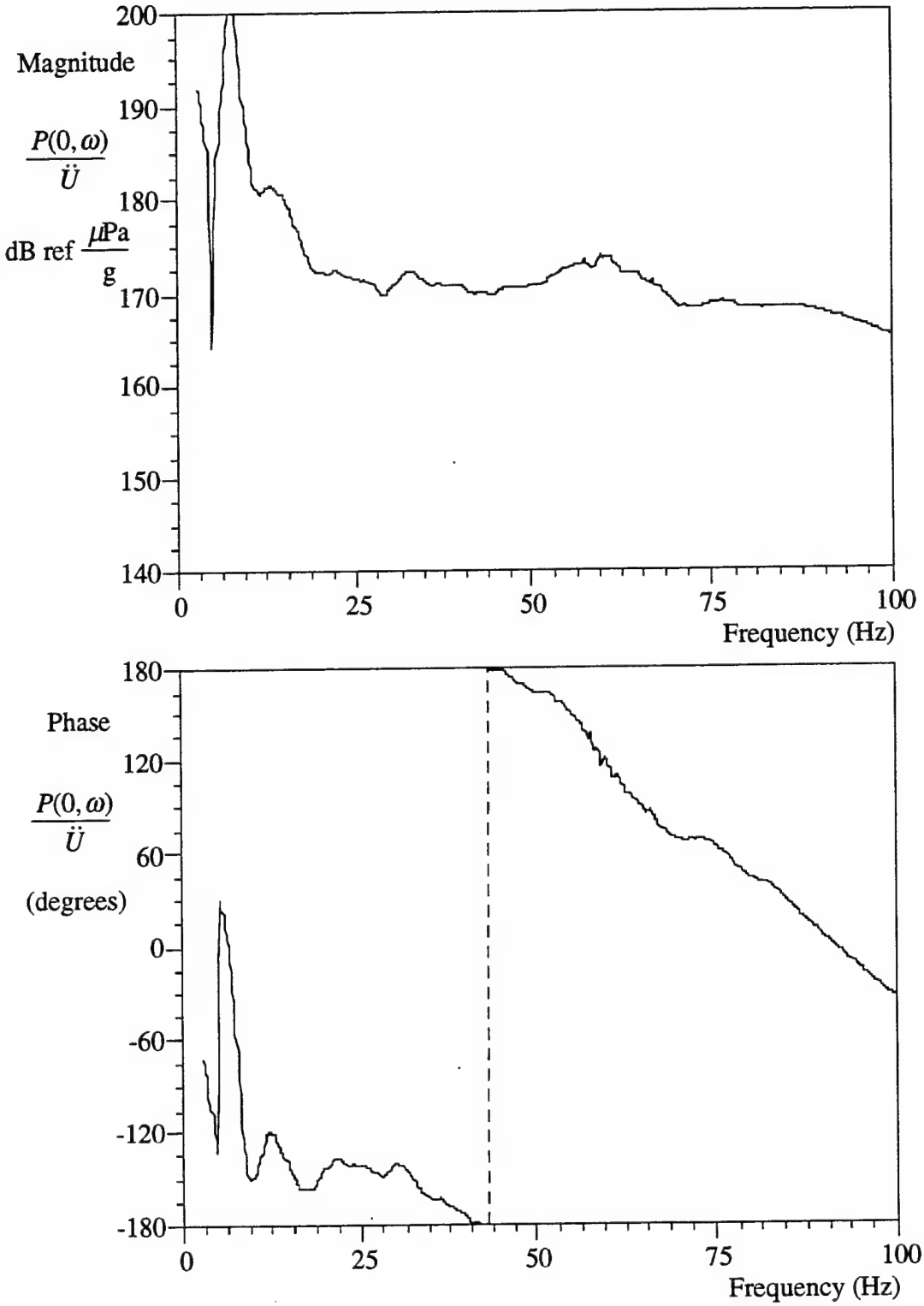

Figure 7. Third Hydrophone Pressure Divided by Forward Acceleration Versus Frequency

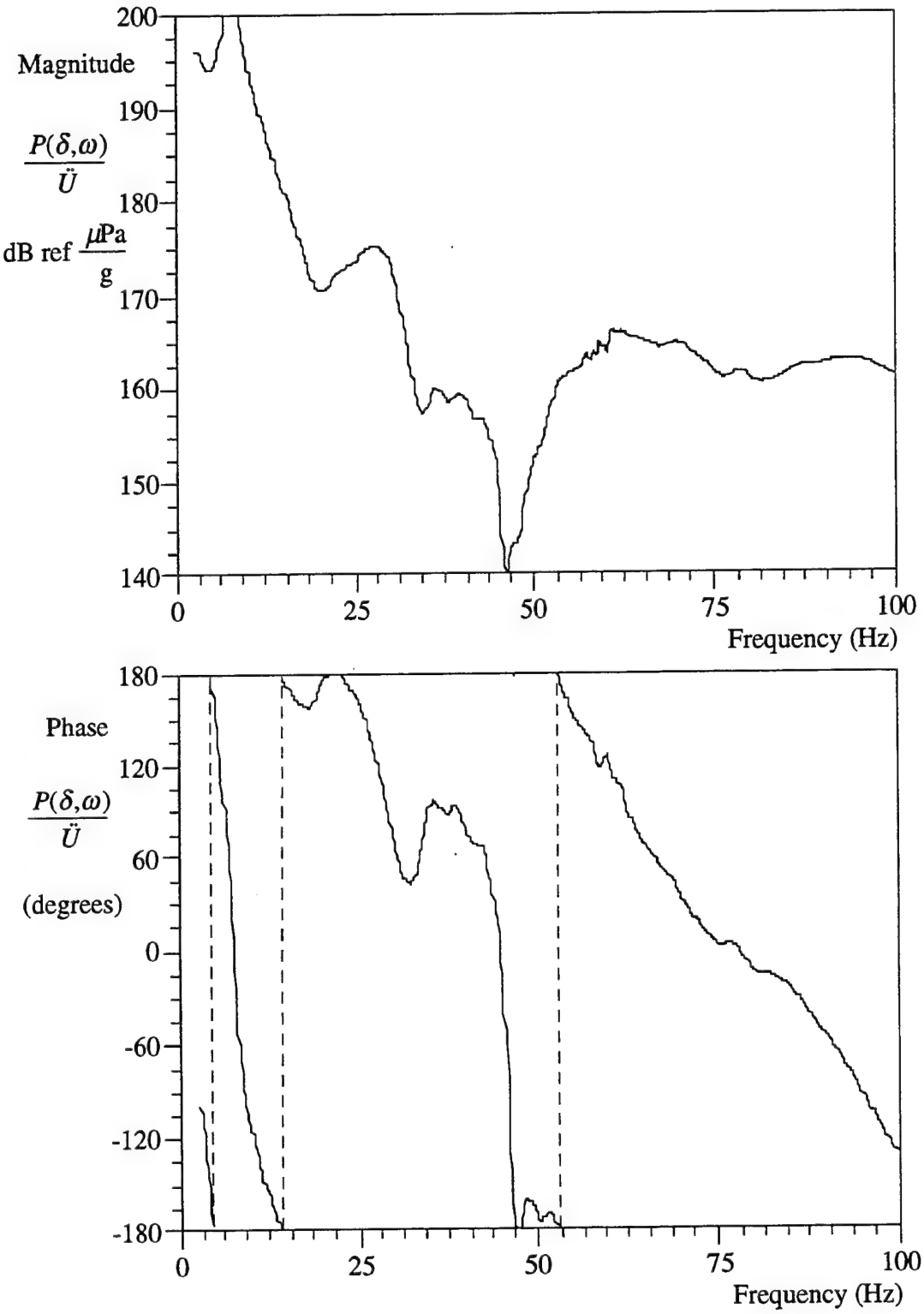

Figure 8. Fourth Hydrophone Pressure Divided by Forward Acceleration Versus Frequency

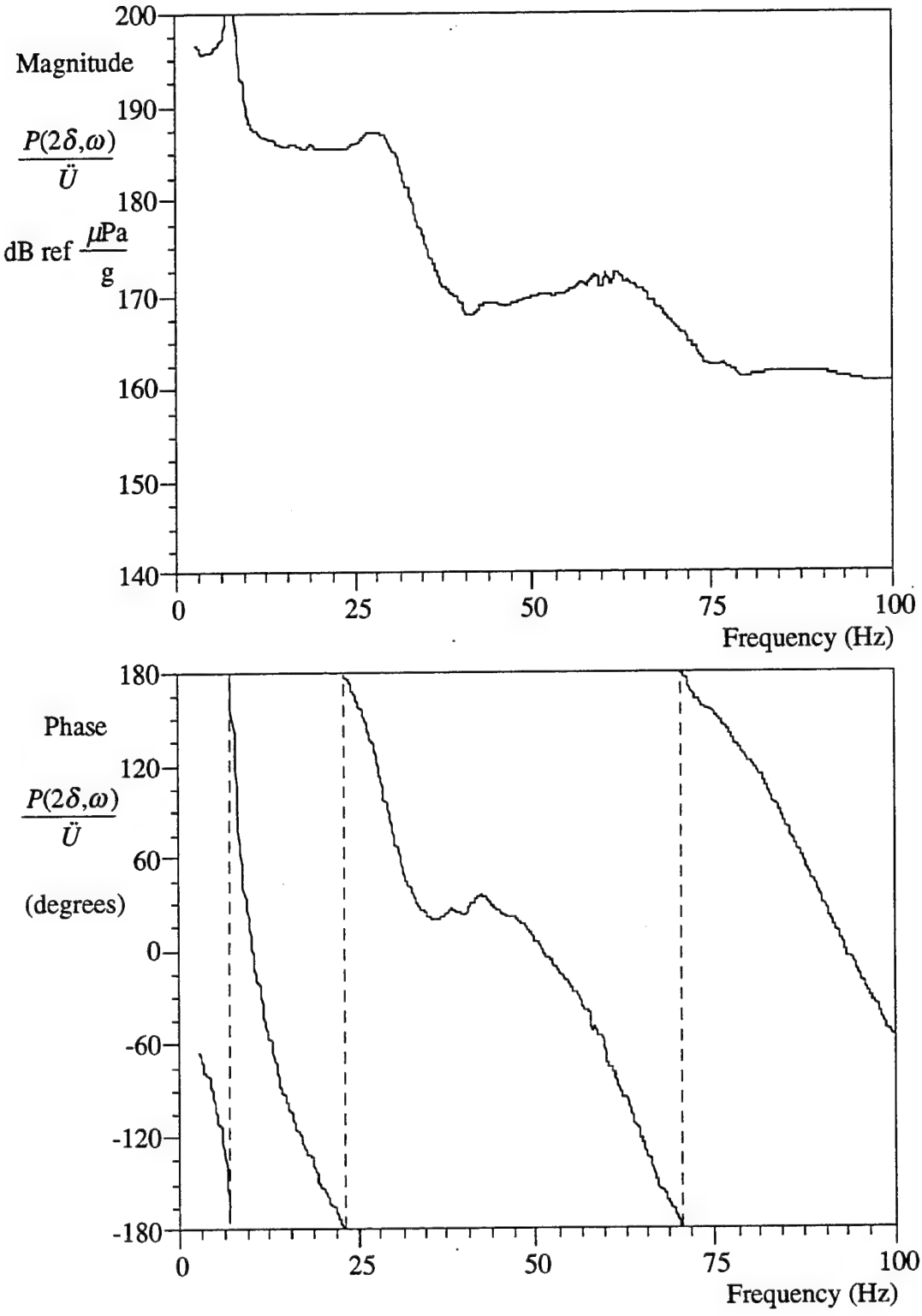

Figure 9. Fifth Hydrophone Pressure Divided by Forward Acceleration Versus Frequency

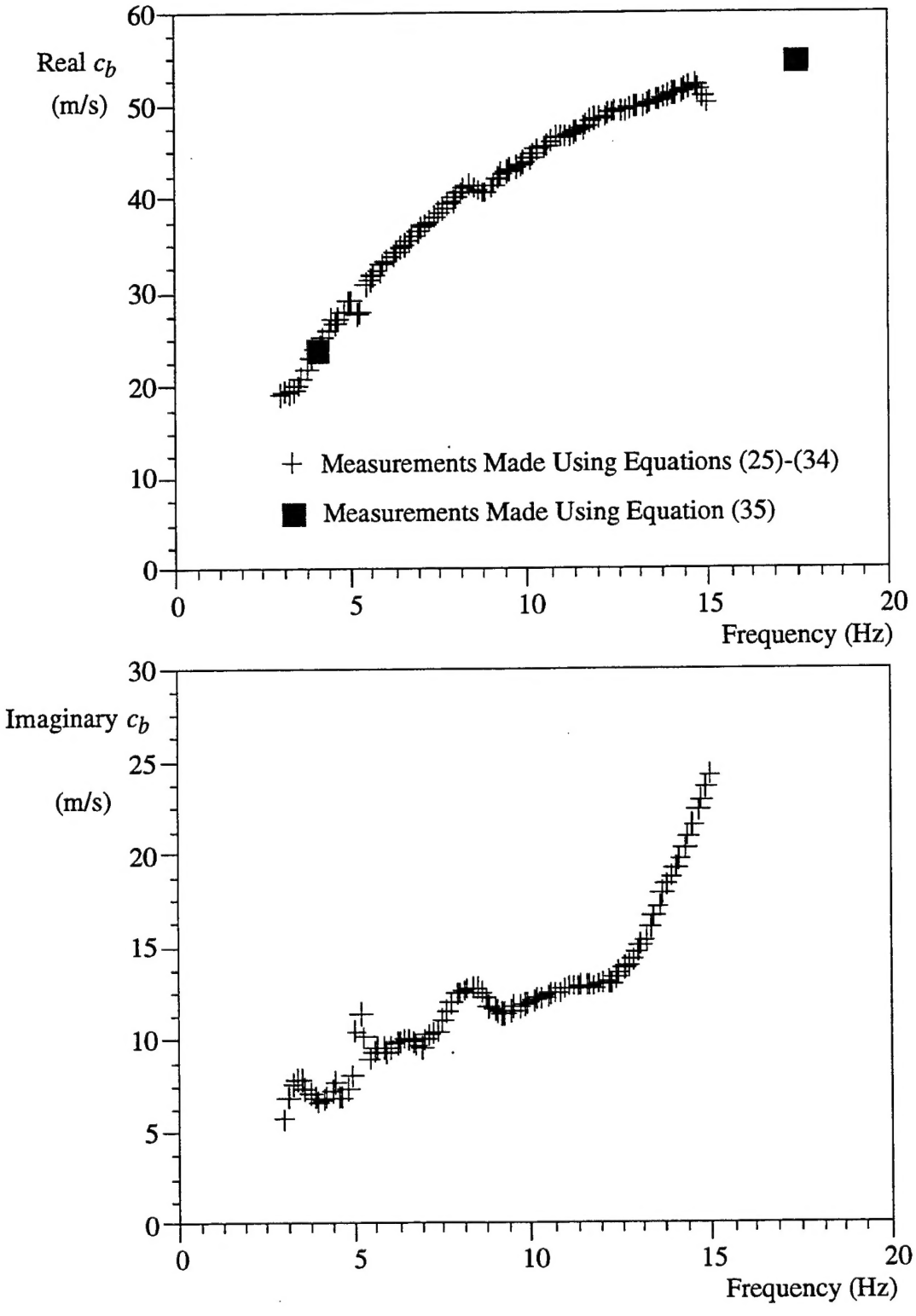

Figure 10. Breathing Wave Speed Versus Frequency

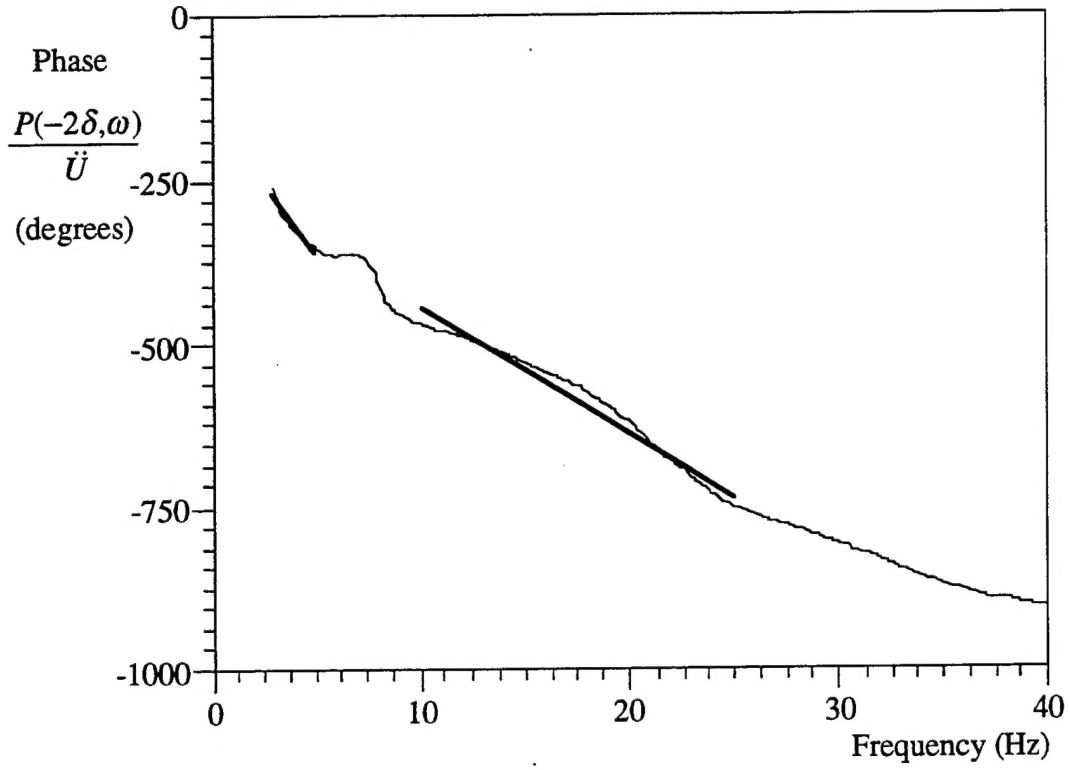

Figure 11. First Hydrophone Phase Angle With Straight-Line Fits

5. CONCLUSIONS

The breathing wave speed of a liquid-filled shell can be determined with five equally spaced hydrophones. This technique separates the spatial pressure field into two waves: an extensional wave and a breathing wave. First, the extensional wave speed is determined using force transducers and accelerometers located at the ends of the shell. Next, the breathing wave speed is calculated using measurements from the hydrophones and the extensional wave speed measurement. The method yields a complex value at every frequency for which data are collected and for which the breathing wave is spatially coherent. This test can be run very rapidly, and the corresponding computations are not intensive.

6. REFERENCES

1. M. C. Junger and D. Feit, 1986, *Sound, Structures, and Their Interaction*, The MIT Press, Cambridge, Massachusetts, pp. 37-40.

2. A. J. Hull, 1994, "A Technique to Measure the Breathing Wave Speed in a Towed Array," *Journal of Vibration and Acoustics*, Vol. 116, No. 2, pp. 243-245.

3. A. J. Hull, 1996, "An Inverse Method to Measure the Axial Modulus of Composite Materials Under Tension," *Journal of Sound and Vibration* (To Be Published).

INITIAL DISTRIBUTION LIST

Addressee	No. of Copies
Defense Technical Information Center	12
Naval Sea Systems Command (CAPT G. Kent, PMS-425; M. Basilica, Code 4251; D. Lechner, PMS-42511)	3
Office of Naval Research (ONR 321: T. G. Goldsberry, K. Dial, R. Varley)	3
Program Executive Office-USW-ASTO (CDR J. Polcari, W. Chen, A. Hommel, J. Jones, LCDR M. Traweek, R. Melusky)	6
Space and Naval Warfare System Command (J. P. Feuillet, PMW-182)	1
Michigan State University (C. R. MacCluer, C. J. Radcliffe)	2
Applied Measurement Systems, Inc. (J. Diggs, R. Hauptmann)	2
Cambridge Acoustical Associates, Inc. (J. E. Cole, J. M. Garrelick)	2
Technology Service Corporation (L. W. Brooks)	2